

University of Nebraska - Lincoln

DigitalCommons@University of Nebraska - Lincoln

Department of Chemical and Biomolecular
Engineering: Faculty Publications

Chemical and Biomolecular Engineering,
Department of

9-20-2023


Conduction Mechanism Switching from Coulomb Blockade to Classical Critical Percolation Behavior in Disordered Nanoparticle Array

Abhijeet Prasad

Jay Min Lim

Ravi Saraf

Follow this and additional works at: <https://digitalcommons.unl.edu/chemengall>

 Part of the [Biochemical and Biomolecular Engineering Commons](#), and the [Biomedical Engineering and Bioengineering Commons](#)

This Article is brought to you for free and open access by the Chemical and Biomolecular Engineering, Department of at DigitalCommons@University of Nebraska - Lincoln. It has been accepted for inclusion in Department of Chemical and Biomolecular Engineering: Faculty Publications by an authorized administrator of DigitalCommons@University of Nebraska - Lincoln.

Conduction Mechanism Switching from Coulomb Blockade to Classical Critical Percolation Behavior in Disordered Nanoparticle Array

Abhijeet Prasad, Jay Min Lim, and Ravi F Saraf^{*}

Large, open-gate transistors made from metal nanoparticle arrays offer possibilities to build new electronic devices, such as sensors. A nanoparticle necklace network (N^3) of Au particles from 300 K to cryogenic temperatures exhibit a nonohmic $I-V_d$ behavior, $I \approx (V_d - V_T)^\zeta$, where V_T is a conduction gap and ζ is a constant critical exponent. The conduction gap in N^3 , made from disordered networks of 1D chains of 10 nm diameter Au particles exhibits room temperature (RT) gating. Although the $I-V_d$ behavior at RT is identical to Coulomb blockade, the conduction is modulated by field-assisted tunneling exhibiting classical critical behavior. In this study, based on three results, invariance of V_T on gating, invariance of V_T on temperature, and zero-bias conductance, a sharp transition temperature at ≈ 140 K is discovered where the conduction mechanism switches from Coulomb blockade to classical critical percolation behavior. The N^3 architecture allows the reconciliation of the Coulomb blockade versus activation process as a sharp thermal transition to serve as a model system to study the exotic behavior in nanogranular-metallic materials. The novel global critical behavior to local Coulomb blockade governed transition in these N^3 architectures may potentially lead to novel sensors and biosensors.

ordered arrays of metallic nanoparticles/nano-islands has been studied for over six decades because of their potential to develop highly sensitive single electron transistors.^[17] These arrays typically show a metal-to-insulator transition at cryogenic temperatures (T) where the electron transport below a conduction gap, V_T is inhibited due to local charging at multiple sites by just a single electron, causing an electrostatic barrier referred to as Coulomb blockade (CB) effect,^[18,19] which is sensitive to both the size of the particles^[20,21] as well as the length of the array.^[5,6,22] The consequence is critical behavior like electron transport characteristics where the current, I , as a function of applied bias, V_d across the array is given by, $I \approx (V_d - V_T)^\zeta$ where, V_T is a conduction gap and ζ is a critical scaling exponent.^[23] There have been numerous studies at cryogenic temperatures that show CB in metal nanoparticle arrays.^[2,22,24–26] Recently, a disordered network of 1D 10 nm

diameter Au nanoparticle chains, referred to as nanoparticle necklace networks (N^3) was shown to exhibit functionally identical behavior $I-V_d$ as Coulomb blockade at room temperature (RT).^[27–30] Using image analysis of N^3 morphology by Scanning Electron Microscope (SEM),^[30] the origin of the identical scaling $I-V_d$ behavior at RT was shown to be an electric field assisted tunneling activated classical critical (CC) behavior due to self-similar growth of percolation paths in the network as V_d is increased.^[31] The structure of N^3 was shown to have hierarchical morphology where the growth of percolation path grows in a (self-similar) fractal dimension.^[31] In this model, the threshold V_T for conduction is the bias for percolation to commence and the nonlinear growth for $V_d > V_T$ is opening up of more percolation paths in the conducting network regulated by the activated process of field-assisted tunneling rather than CB effect.^[31] Thus, the emergence of V_T in N^3 at RT depends on the global architecture (i.e., CC behavior), rather than local charging (i.e., CB effect).


Dense, ordered metallic nanoparticle array transistors can be gated due to the charging of nanoparticles, which modulates the CB effect. This modulation, however, rapidly vanishes at T above 100 K, because electrons have enough thermal energy to overcome the CB barriers.^[6,22,26,32] The N^3 exhibits gating at RT. When

1. Introduction

Arrays of metal nanoparticle arrays have been of great interest for their unique electronic,^[1–9] optical^[10–12] and electrochemical^[13–16] properties and the ability to self-assemble them to make practical devices. The conduction gap that occurs in

A. Prasad, J. M. Lim, R. F Saraf
Department of Chemical and Biomolecular Engineering
University of Nebraska-Lincoln
207 Othmer Hall, Lincoln, NE 68588, USA
E-mail: rsaraf2@unl.edu

R. F Saraf
Nebraska Center for Materials & Nanoscience
Voelte-Keegan Nanoscience Research Center
N201 NANO, Lincoln, NE 68588, USA

 The ORCID identification number(s) for the author(s) of this article can be found under <https://doi.org/10.1002/aelm.202300485>

© 2023 The Authors. Advanced Electronic Materials published by Wiley-VCH GmbH. This is an open access article under the terms of the Creative Commons Attribution License, which permits use, distribution and reproduction in any medium, provided the original work is properly cited.

DOI: 10.1002/aelm.202300485

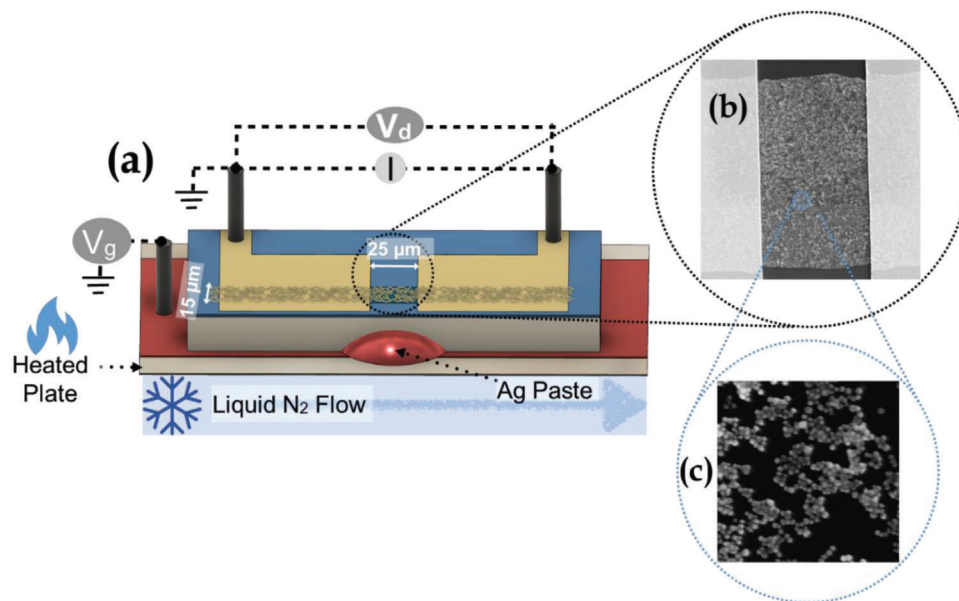


Figure 1. Schematic of the device. a) The device consists of two ≈ 100 nm thick gold pads on ≈ 10 nm thick silica gate oxide layer separated by a $25 \mu\text{m}$ gap. The gold pads are bridged by a $15 \mu\text{m}$ wide channel of N^3 . Gating experiments were conducted by connecting a silver paste to the bottom silicon layer on a temperature-controlled plate. (b) and (c) are Scanning Electron Microscope (SEM) images of N^3 .

a positive gating potential, V_g , is applied to N^3 transistors, there is a rise in the Fermi level that causes isolated clusters to connect to the network, which increases the array conductivity.^[31] Unlike in CB-mediated transistors, V_T and ζ remain invariant with respect to gating potential, V_g , leading to a universal $I-V_d$ behavior.^[31] Although the mesoscale geometry of N^3 is markedly different from dense arrays, both devices share a similar nanoscale structure with metallic nanoparticles separated by small gaps, typically, below 1 nm; and their $I-V_d$ characteristics $I \approx (V_d - V_T)^\zeta$ are identical. It is therefore, expected that, below a certain temperature, N^3 should also exhibit CB effect. Here, we examine the CC to CB behavior as the temperature is lowered.

We discovered that N^3 exhibits a sharp transition temperature, T_C from CC to CB behavior. We found three orthogonal evidences

consistently showing a T_C at ≈ 140 K. First, V_T remains invariant at $T > T_C$ (attributed to tunneling-mediated CC behavior that is temperature independent)^[31] then rapidly increases below T_C as expected due to CB effect.^[2] Second, for $T > T_C$, V_T is independent of V_g (attributed to CC percolation behavior)^[31] followed by a rapid increase in V_g dependence as temperature drops below T_C marking the commencement of CB effect. Third, the zero-bias conductance behaviors show a (very) sharp transition from activated CC behavior ($T > T_C$) to CB behavior ($T < T_C$). The unique conduction mechanisms in these N^3 arrays and well-established surface modification methods on Au opens a range of exciting opportunities to develop highly sensitive large-area open gate field effect transistors (ogFET) for chemical sensors, immunospecific biosensors, water splitting electrode, and living transistors.^[33–36]

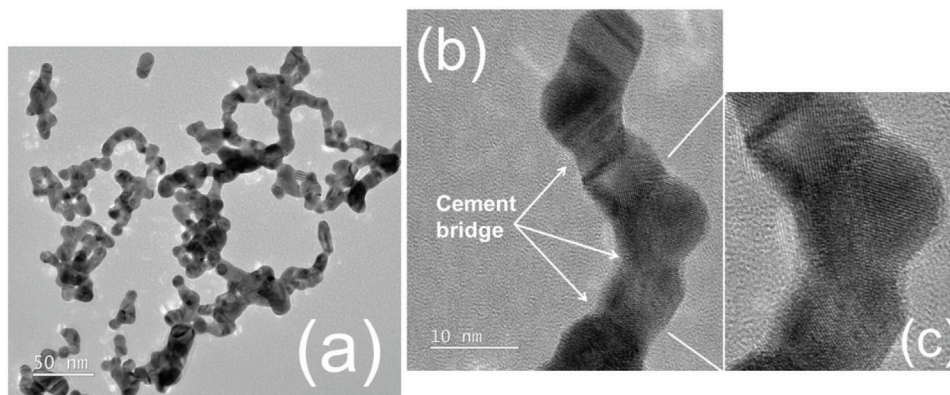


Figure 2. Structure of cemented Au nanoparticle necklaces. a) TEM image of the Au nanoparticle chains after the nanocement process. b) Higher magnification shows the nanocement between the nanoparticles. c) The lattice planes are visible in the high-resolution images showing polycrystalline structure with no specific interparticle orientation. (Image 2c is an independent image from 2b of the same region).

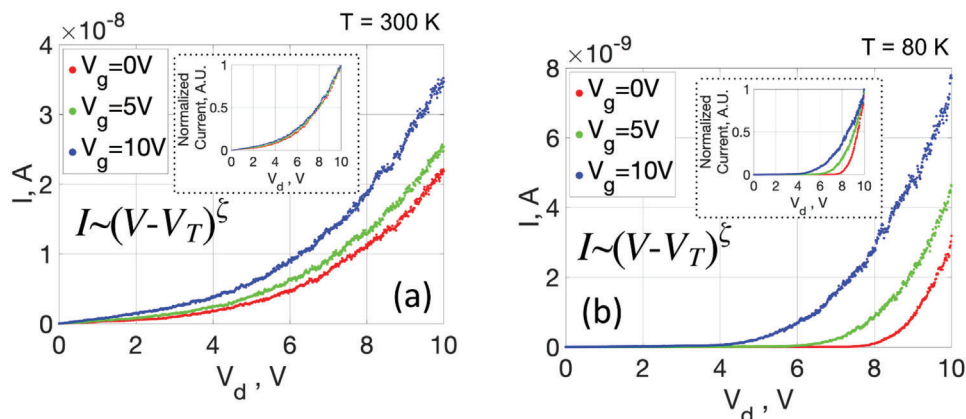


Figure 3. The gating behavior. a) The I - V_d behavior of N^3 at 300 K for $V_g = 0, 5,$ and 10 V. A $V_T = 1.08$ V for all three curves was obtained, with minimum fitness $R^2 = 0.978$. The invariant V_T led to universal behavior (see inset). b) The I - V_d behavior at 80 K for $V_g = 0, 5,$ and 10 V. The V_T obtained was $7.12, 5.29,$ and 3.07 V for $V_g = 0, 5,$ and 10 V, respectively. The minimum fitness for the three curves was $R^2 = 0.98$.

2. Results and Discussion

The Au nanoparticles were synthesized (Section S1, Supporting Information) with a reasonably sharp particle size distribution of 9.73 ± 0.816 nm as measured by image analysis (Section S2, Supporting Information). The particles have a face-centered cubic crystal structure as observed by x-ray diffraction and high-resolution Transmission Electron microscopy (HRTEM) (Section S3, Supporting Information). The orientation and grain structure due to (111) lattice plane fringes in HRTEM show that the particles are polycrystalline (Figure S7b, Supporting Information). The 1D nanoparticle chains were formed by adding $CaCl_2$ salt to bridge 10 nm citrate stabilized Au nanoparticles to form 1D chains, similar to the previously described nano-cementing process.^[27,28] The necklace formation was conveniently monitored by UV-vis spectra of the nanoparticle suspension that broadens as the particles aggregate to form 1D chains (Section S4 and Figure S8, Supporting Information). Next, the device was fabricated as described in a previous publication^[31] and in (Section S5, Supporting Information). The process had five broad steps: First, the 100 nm thick thermal oxide between the Au electrodes was etched to ≈ 10 nm to form the gate oxide (See Section

S5 (Supporting Information) subsection Gate Oxide Formation). Thin gate oxide was necessary to increase the gate capacitance to cause effective (local) charging of N^3 on application of V_g . Second, a 15 μm wide, 25 μm long channel of 3-aminopropyl triethoxysilane (APTES) was patterned between the electrodes in a multi-step process using photolithography as described in a previous publication^[31] (also see, Section S5 and Figure S9, Supporting Information). Third, the negatively charged nanoparticle necklaces were selectively deposited on the positively charged APTS channel (Figure 1b). Owing to the negative charge of the necklaces, the resulting morphology was a self-limiting monolayer of necklaces forming N^3 morphology (Figure 1c). Fourth, the chip with deposited N^3 was immersed in a 1 M Na_2CO_3 to form a “nanocement” of calcium carbonate (Figure 2). The nanocement served as a barrier for both tunneling and electromigration. Fifth, the Si substrate was etched to expose the thin oxide layer from the bottom, which was subsequently interconnected via conductive silver paste from the gating electrode. To note that Au nanoparticle surface is not significantly contaminated/affected during necklace formation and N^3 fabrication, due to the cementing. Nano-cementing Au nanoparticle necklaces with CdS in N^3 structure leads to a strong electroluminescence with appropriate EL

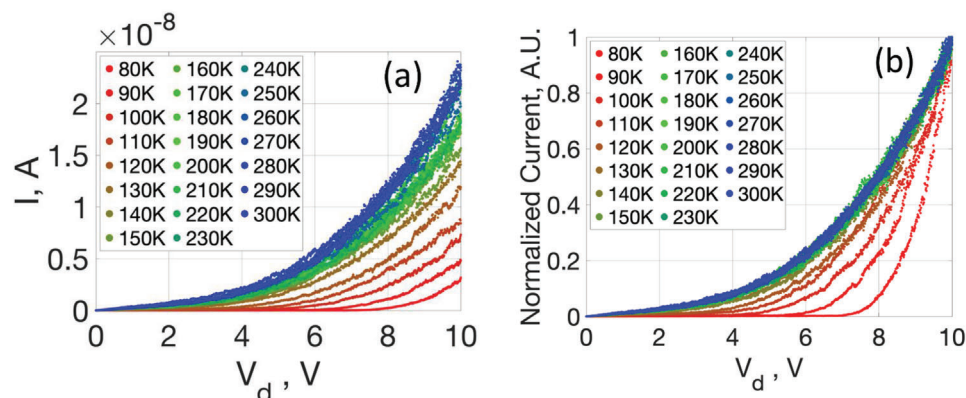


Figure 4. Thermal behavior. a) The I - V_d behavior as T decreases from 300 to 80 K. b) After normalization of I with respect to current at $V_d = 10$ V.

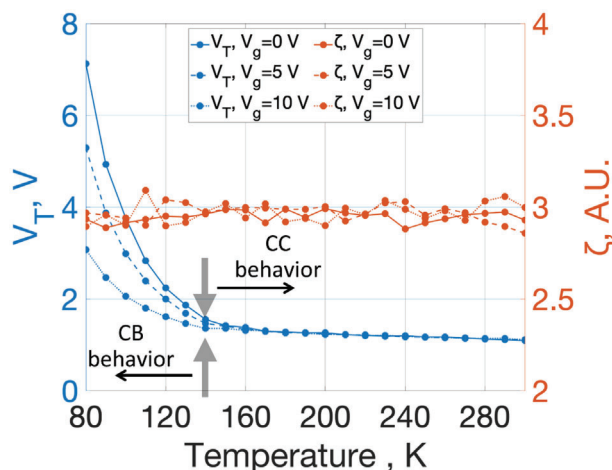


Figure 5. The two regimes of electron transport. V_T and ζ as a function of temperature for $V_g = 0, 5,$ and 10 V. V_T behavior shows a critical temperature at which universality breaks down and V_T changes with both temperature and V .

spectrum indicating the formation of a barrier of the CdS with excellent interconnection along the percolation path.^[28]

Typical $I-V_d$ characteristics of N^3 at 300 and 80 K show the same power law behavior, $I \approx (V_d - V_T)^\zeta$ with a well-defined V_T and ζ at minimum fitness, R^2 of 0.98 (Figure 3). For $T = 300$ K, as a positive V_g is applied the I rises (Figure 3a). Remarkably, the V_T remains invariant and all the curves at different V_g collapse into a single universal curve (inset, Figure 3a). The invariance of V_T is consistent with CC behavior shown previously over a larger range of 25 V.^[31] The rise in current is attributed to a local shift in the Fermi levels of isolated nanoparticle chains to cause additional chains to connect to the percolating paths increasing the network density. The invariance in V_T with respect to V_g leads to CC behavior.^[31] Although the $I-V_d$ behavior is unchanged at lower temperature (Figure 3b), the universality with respect to V_g

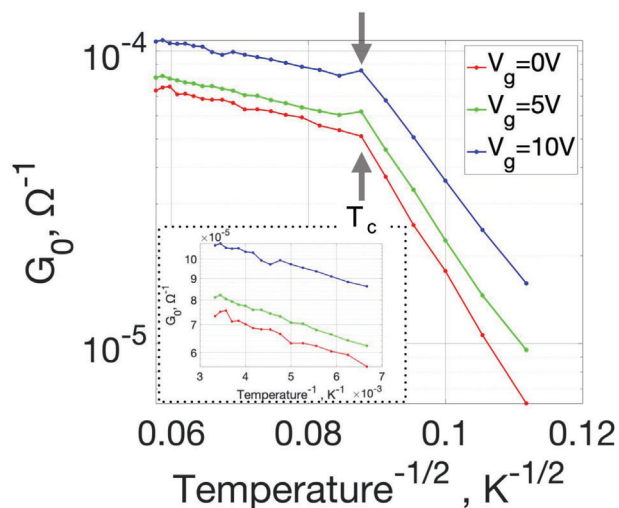


Figure 6. Zero-Bias Conductance. Zero-bias conductance showing cotunneling behavior with $G_0 \propto T^{-0.5}$ below T_C while showing Arrhenius behavior at $T > T_C$ (inset).

vanishes. The V_T decreases as V_g increases (inset, Figure 3b). The modulation in V_T due to V_g signifies the CB effect.^[13] Therefore, the mechanism of electron signport at 300 and 80 K is fundamentally different.

Unlike in bulk metals, as T is decreased from 300 to 80 K, the current drops monotonically (Figure 4a). The decrease in I at $V_d \approx 8$ V is more than an order of magnitude. On normalizing the current with respect to I at $V_d = 10$ V, it is clear that at higher temperatures, $T > 140$ K, $I-V_d$ V_T is constant, i.e., universal behavior (Figure 4b). This is consistent with the previously described CC behavior.^[31] In CC regime, the conduction network grows in a self-similar fractal dimension as the bias increases to cause larger inter-particle distance to become part of the conducting network due to field-assisted tunneling.^[31] This growth of percolation pathways with increasing bias is characterized by threshold potential, V_T . As this nonlinear $I-V_d$ emerges from tunneling hierarchy, which is T independent, the critical point, V_T in the CC regime is expected to be independent of T . We note in passing, there is linear background current that is evident at $V < V_T$ due to few percolation channels that span over the whole distance with interparticle distance below ≈ 1 nm (Section S6 and Figure S10, Supporting Information). In low-temperature regime, $T < 140$ K, the V_T begins to increase as T decreases. This is due to the CB effect. As the thermal energy of conduction electrons lowers due to decreasing T , the number of CB barriers increases leading to a larger V_T . Thus, the transition from CC to CB is at $T_C \approx 140$ K.

Figure 5 shows the change in the V_T and ζ as a function of T . From 300 to ≈ 140 K, for a fixed V_g , the V_T is nominally constant with a slow linear increase. This signifies CC behavior.^[31] For T below ≈ 140 K, the V_T begins to rapidly increase nonlinearly signifying the CB regime. The transition temperature, T_C , from the (slow) linear increase in V_T to the commencement of rapid nonlinear rise was determined by linear regression analysis to obtain, $T_C = 140$ K (see details in Section S7, Supporting Information). For $T < T_C$ the V_T rapidly rises at 140 K indicating the CB regime, while for $T > T_C$ the slope of V_T versus T is -1.5 mV K^{-1} . The rapid rise in the CB regime amounts to ≈ 6.5 fold increase in V_T over 70 K. The dependence of V_T on T in the CB regime is consistent with the CB characteristics observed a low temperatures for a dense array of nanoparticles^[2,26] and for N^3 .^[37] For reasons unknown to us then, the trend of rapid drop in V_T at low temperatures followed by an invariant behavior was observed before for a different N^3 morphology with no nano-cementing.^[37] Thus, the sharp CB to CC transition observed in N^3 is fairly general which primarily depends on its unique morphology of local 1D architecture. Considering the tail of Fermi-Dirac statistics, it is reasonable to expect that electrostatic barrier height should be higher than ≈ 3 kT to observe CB effect.^[38] Typical charging energy of 10 nm Au particle is ≈ 50 meV. Thus, the barrier height at T_C of roughly four times the thermal energy is consistent with the electrostatics of N^3 . The second strong corroborating evidence for CC to CB transition at $T_C \approx 140$ K is the gating behavior. From the previous observation, in the CC regime, the V_T is independent of V_g spanning over 25 V.^[31] It is clearly evident in Figure 5 that for $T > T_C$ the V_T is independent of V_g while for $T < T_C$ a dependence on V_g commences. Thus, T_C is a transition temperature from CC to CB regime (Figure 5). The third evidence of the conduction mechanism switching from CC to CB behavior is by measuring the zero-bias conductivity (G_0). The T dependence on

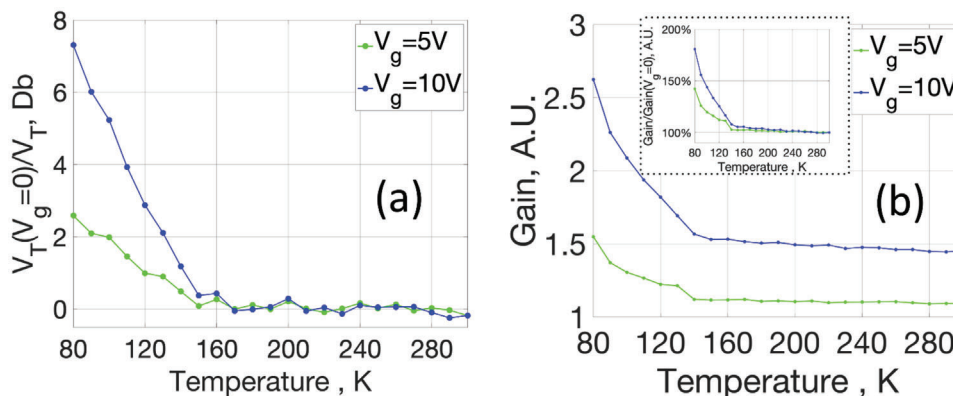


Figure 7. a) Ratio of $V_T(T)/V_T(T = 300\text{ K})$ for $V_g = 0, 5,$ and 10 V . At $V_g = 10\text{ V}$ this increase in V_T can be higher than 700% compared to 300 K . b) Changing gain as a function of temperature. As a result of changing V_T the gain can change more than 150% at $V_g = 10\text{ V}$ (inset).

G_0 in the low bias regime ($V_d < V_T$) for granular systems can be derived from multiple co-tunneling theory as^[24]:

$$G_0(T) \propto \exp(-T^\nu) \quad (1)$$

where $\nu = -\frac{1}{2}$ in the presence of CB. The exponent ν is experimentally verified at low temperatures in CB regime.^[24] At high temperatures the co-tunneling vanishes and the $\nu = -1$.^[22] The $\nu = -1$ is attributed to simple Arrhenius-type activated behavior.^[39] For N^3 , G_0 shows a sharp change around T_C (Figure 5). For $T > T_C$ $\nu = -1$, see Figure 6 (inset). This indicates that transport governed by field-assisted tunneling in CC behavior regime is an activated Arrhenius-type process. For $T < T_C$, least squares best fit matches closely to $\nu = -\frac{1}{2}$, consistent with co-tunneling behavior in CB regime.^[24]

The $T_C \approx 140\text{ K}$ for CB to CC transition is remarkably sharp. This may be explained as follows: The potential CB sites are spatially fixed (due to a large tunneling barrier or quenched charge in the substrate). As T decreases below T_C the CB barrier density monotonically increases due to the lower thermal energy of the free electron, thus, V_T is a strong function of T . Above T_C all the potential CB barrier, i.e., “isolated” particles, are removed. They only pose tunneling barriers based on the inter-particle gap.^[31] These barriers can be overcome by field-assisted tunneling. Thus, the percolation network grows as bias increases.^[31] As the tunneling barrier in the hierarchical percolating network is expected to be independent of temperature, in the CC regime the dependence of V_T on T is weak. Thus, the origin of the nonlinear behavior in the two regimes is very different. Interestingly, the scaling exponent, ζ , remains constant (Figure 5) with T and V_g , indicating that changes in the charging energy do not alter the fractal percolation network topology.

As a transistor for applications, the conduction mode of N^3 has implications on the resulting gain and therefore the sensitivity of the device. At temperatures below T_C applying V_g causes the V_T to decrease. As a result, the gain is a factor of ≈ 7 at $V_g = 10\text{ V}$, $T = 80\text{ K}$ (Figure 7a). The shift in V_T causes the gain to be much higher at lower temperatures in CB regime than in CC regime. However, in the CC regime the gain is nominally temperature-independent.

3. Conclusion

Low-temperature electronic behavior of nanoparticle necklace networks (N^3), an array of 2D random networks of 1D chains of 10 nm Au nanoparticles were studied. A nonohmic $I-V_d$ given by $I \approx (V_d - V_T)^\zeta$ was observed at a fitness of $R = 0.99$ for $T = 80$ to 300 K . Unlike bulk metals, the conductivity decreased with T . For identical $I-V_d$ characteristics, two distinct conduction mechanism regimes were observed with a sharp transition at $T_C \approx 140\text{ K}$. The transition temperature, T_C between the two regimes was consistent among three orthogonally different characteristics: i) For $T > T_C$, the V_T remained constant while below T_C the V_T increased rapidly as T was decreased. ii) For $T > T_C$, the V_T is invariant as a function of V_g while below T_C the V_T increases as V_g increases. iii) The exponent ν in $G_0 \approx \exp(-T^\nu)$, for $T > T_C$, is -1 while below T_C sharply changes to $-1/2$. The above characteristics indicate that a higher temperature regime ($T > T_C$) is an activated process (i.e., $\nu = -1$) where the conduction is mediated by field-assisted tunneling process (i.e., V_T is independent of T) where more percolation paths open as bias increases exhibiting classical critical behavior (i.e., V_T is independent of V_g). Juxtaposed to low-temperature process, for $T < T_C$, the conduction is governed by Coulomb blockade where the barriers are fixed in space allowing co-tunneling (i.e., $\nu = -1/2$) and number density of barriers increases as T decreases (i.e., V_T increases as T decreases) and difficulty to overcome is modulated by gating (i.e., the V_T depends on V_g). The conduction gap V_T at higher temperature ($T > T_C$) is the classical critical point while for lower temperature ($T < T_C$) is cumulative electrostatic Coulomb blockade barriers along the percolation path. Thus, the conduction mechanism of low ($T < T_C$) and high ($T > T_C$) temperature regimes are governed by Coulomb blockade and classical critical behavior, respectively. The remarkable sharpness of the transition indicates that the morphology is of CB barriers and the hierarchy of tunneling gap distribution over the 20 by $25\text{ }\mu\text{m}$ array is uniform. Interestingly, and not understood is that the critical exponent, ζ remains constant over the whole temperature range studied. The sharp transition between the two modalities governed by local and global structure in N^3 architecture (not observed in dens array of nanoparticles²) can serve as a powerful model system to learn new exotic physics of charge transport in granular systems,

especially in large random networks where the topology can be tailored and quantified to potentially alter $I-V_d$ properties including T_C .

4. Experimental Section

Nanoparticle Synthesis, N³ Fabrication, and Structure Characterization: The nanoparticle synthesis and N³ fabrication are described in Sections S1, S4 and S5 (Supporting Information), respectively. The nanoparticle characterization is described in Sections S2 and S3 (Supporting Information).

Electrical Characterization: The bottom of the chip was stripped of oxide for a second time using 1% hydrofluoric acid. Once the Si surface was exposed, the chip was bonded to a silver conductive paste to apply the gate potential. After bonding, the chip was installed inside a Lakeshore Cryogenics ST-500 probe station, where contact was made to source, drain, and gate electrodes by tungsten pins. The probe station was pumped down to a vacuum below 10⁻⁶ Torr and the sample was allowed to rest under vacuum for 30 min before taking electrical measurements. The T was controlled using a Lakeshore Cryogenics Model 336 temperature controller with liquid nitrogen flow. Electrical properties of the N³ ogFET were characterized using a Keithley 4200A-SCS Parameter Analyzer. The bias was applied at a step size of 10 mV across the source and drain or source and gate with the drain grounded while the current was measured.

Supporting Information

Supporting Information is available from the Wiley Online Library or from the author.

Acknowledgements

R.F.S. would like to thank the US Army Research Office (W911NF-21-1-0224 and W911NF-23-1-0036) for financial support.

Conflict of Interest

The authors declare no conflict of interest.

Data Availability Statement

The data that support the findings of this study are available from the corresponding author upon reasonable request.

Keywords

coulomb blockade, critical phenomena, field effect transistor sensors, nanoparticle arrays, neuromorphic devices

Received: July 20, 2023

Revised: September 10, 2023

Published online:

- [1] K. Elteto, X. M. Lin, H. M. Jaeger, *Phys. Rev. B* **2005**, *71*, 205412.
- [2] R. Parthasarathy, X. M. Lin, K. Elteto, T. F. Rosenbaum, H. M. Jaeger, *Phys. Rev. Lett.* **2004**, *92*, 076801.
- [3] V. Gasparian, U. Simon, *Phys B Condens Matter* **1997**, *240*, 289.
- [4] U. Simon, *Adv. Mater.* **1998**, *10*, 1487.
- [5] Y. Cai, J. Michels, J. Bachmann, C. Klinke, *J. Appl. Phys.* **2013**, *114*, 034311.
- [6] M. Galchenko, A. Black, L. Heymann, C. Klinke, *Adv. Mater.* **2019**, *31*, 1900684.
- [7] T. A. Fulton, G. J. Dolan, *Phys. Rev. Lett.* **1987**, *59*, 109.
- [8] L.-C. Tsai, I. C. Cheng, M. C. Tu, C. D. Chen, H.-Y. Lin, *J Nanopart Res* **2010**, *12*, 2859.
- [9] K.-H. Müller, J. Herrmann, B. Raguse, G. Baxter, T. Reda, *Phys. Rev. B* **2002**, *66*, 075417.
- [10] Y. Chu, E. Schonbrun, T. Yang, K. B. Crozier, *Appl. Phys. Lett.* **2008**, *93*, 181108.
- [11] Z. Zhan, R. Xu, Y. Mi, H. Zhao, Y. Lei, *ACS Nano* **2015**, *9*, 4583.
- [12] A. Ghoshal, P. G. Kik, *J. Appl. Phys.* **2008**, *103*, 113111.
- [13] S. W. Lee, E. H. Lee, R. F. Saraf, *ChemElectroChem* **2014**, *1*, 1281.
- [14] Y.-G. Zhou, S. Yang, Q. Y. Qian, X. H. Xia, *Electrochem. Commun.* **2009**, *11*, 216.
- [15] R. W. Murray, *Chem. Rev.* **2008**, *108*, 2688.
- [16] D. Lantiat, V. Vivier, C. Laberty-Robert, D. Grosso, C. Sanchez, *ChemPhysChem* **2010**, *11*, 1971.
- [17] K. Likharev, *IEEE T Magn* **1987**, *23*, 1142.
- [18] U. Geigenmüller, G. Schön, *Europhys Lett* **1989**, *10*, 765.
- [19] J. Lambe, R. C. Jaklevic, *Phys. Rev. Lett.* **1969**, *22*, 1371.
- [20] Y. Zhang, O. Pluchery, L. Caillard, A. F. Lamic-Humblot, S. Casale, Y. J. Chabal, M. Salmeron, *Nano Lett.* **2015**, *15*, 51.
- [21] D. Davidovic, M. Tinkham, *Appl. Phys. Lett.* **1998**, *73*, 3959.
- [22] H. Lehmann, S. Willing, S. Möller, M. Volkmann, C. Klinke, *Nanoscale* **2016**, *8*, 14384.
- [23] A. A. Middleton, N. S. Wingreen, *Phys. Rev. Lett.* **1993**, *71*, 3198.
- [24] T. B. Tran, I. S. Beloborodov, X. M. Lin, T. P. Bigioni, V. M. Vinokur, H. M. Jaeger, *Phys. Rev. Lett.* **2005**, *95*, 076806.
- [25] K. C. Beverly, J. F. Sampaio, J. R. Heath, *J. Phys. Chem. B* **2002**, *106*, 2131.
- [26] F. Remacle, K. C. Beverly, J. R. Heath, R. D. Levine, *J. Phys. Chem. B* **2003**, *107*, 13892.
- [27] V. Maheshwari, J. Kane, R. F. Saraf, *Adv. Mater.* **2008**, *20*, 284.
- [28] J. K. Y. Ong, C. V. Nguyen, S. Sayood, R. F. Saraf, *ACS Nano* **2013**, *7*, 7403.
- [29] C. Yu, S. W. Lee, J. Ong, D. Moore, R. F. Saraf, *Adv. Mater.* **2013**, *25*, 3079.
- [30] P. Wilson, J. K. Y. Ong, A. Prasad, R. F. Saraf, *J. Phys. Chem. C* **2019**, *123*, 19999.
- [31] A. Prasad, M. Stoller, R. F. Saraf, *ACS Appl. Nano Mater.* **2021**, *4*, 9044.
- [32] Y. Suganuma, A.-A. Dhirani, *J. Phys. Chem. B* **2005**, *109*, 15391.
- [33] S. W. Lee, E. H. Lee, G. Thiel, J. L. Van Etten, R. F. Saraf, *ACS Nano* **2016**, *10*, 5123.
- [34] E. H. Lee, S. W. Lee, R. F. Saraf, *ACS Nano* **2014**, *8*, 780.
- [35] H. Fan, V. Maheshwari, *Adv. Mater. Technol.* **2020**, *5*, 2000090.
- [36] H. Fan, V. Maheshwari, *Adv. Funct. Mater.* **2021**, *31*, 2106149.
- [37] J. Kane, M. Inan, R. F. Saraf, *ACS Nano* **2010**, *4*, 317.
- [38] K. Elteto, E. G. Antonyan, T. T. Nguyen, H. M. Jaeger, *Phys. Rev. B* **2005**, *71*, 064206.
- [39] S. Willing, H. Lehmann, M. Volkmann, C. Klinke, *Sci. Adv.* **2017**, *3*, e1603191.